JOURNAL OF GEOPHYSICAL RESEARCH, VOL. 97, NO. E7, PAGES 11,681–11,694, JULY 25, 1992

Voyager 2 Ultraviolet Spectrometer Solar Occultations at Neptune: Constraints on the Abundance of Methane in the Stratosphere

JAMES BISHOP[1] AND SUSHIL K. ATREYA

Department of Atmospheric, Oceanic and Space Sciences, University of Michigan, Ann Arbor

PAUL N. ROMANI

NASA Goddard Space Flight Center, Greenbelt, Maryland

BILL R. SANDEL AND FLOYD HERBERT

Lunar and Planetary Laboratory, University of Arizona, Tucson

Voyager 2 ultraviolet spectrometer (UVS) solar occultation lightcurves at wavelengths 125–138 nm acquired during the Neptune encounter are compared with one-dimensional methane photochemical-transport models. Photoabsorption by methane (the photochemical parent) is expected to be the major source of opacity at these wavelengths, in which case the UVS lightcurves can be used to infer the strength of eddy mixing at altitudes above the methane photolysis peak and compatible CH_4 mixing ratios in the lower stratosphere. For the p-T models adopted in this study, acceptable fits to the UVS lightcurves are obtained with eddy mixing coefficient values ($K_{1/2}$) near the half-light altitudes (placed 550–600 km above the respective 1 bar levels) of $2-15 \times 10^6$ cm^2 s^{-1} (ingress) and $4-35 \times 10^6$ cm^2 s^{-1} (egress) and lower stratospheric ($p > 1.0$ mbar) methane mixing ratio values ($f_T(CH_4)$) of $5-100 \times 10^{-5}$ (ingress and egress). The ranges in $f_T(CH_4)$ and $K_{1/2}$ reflect uncertainties in the background p-T structure and the application of different criteria for deciding what constitutes a "good fit." For the nominal p-T models and a criterion based on replicating the spacing in altitude of the 125–138 nm UVS lightcurves, $K_{1/2}$ values (near 0.2 μbar) of 10^7 cm^2 s^{-1} (ingress) and $1-2 \times 10^7$ cm^2 s^{-1} (egress) and $f_T(CH_4)$ values of $\sim 1 \times 10^{-4}$ (ingress and egress) are indicated, with the egress results being more uncertain. These results are insensitive to photochemical details of the models.

INTRODUCTION

Prior to the Voyager 2 encounter, ground-based measurements of IR emission spectra from Neptune had led to the suggestion that methane was present in the stratosphere of this planet at a mixing ratio of ~2% [*Orton et al.*, 1987, 1990] (see also the review of earlier work by *Orton and Appleby* [1984]). This has been a controversial inference, in that IR radiometry at wavelengths longward of ~15μm pointed to tropopause temperatures 50–55 K near 100 mbar [*Appleby*, 1986; *Orton and Appleby*, 1984] and hence a "cold trap" value for the stratospheric CH_4 mixing ratio in the range $10^{-5}-10^{-4}$. Proposed explanations for a global supersaturation have relied on vigorous convective transport ("moist convective penetration," depositing CH_4 ice particles in the lower stratosphere [*Hunten*, 1974; *Appleby*, 1986; *Lunine and Hunten*, 1989; *Stoker and Toon*, 1989]) from the troposphere where a methane mixing ratio of 2–4% seemed well established [*Baines and Smith*, 1990]. These explanations were speculative, however, in view of our lack of knowledge of basic upper tropospheric parameters (e.g., the temperature lapse rate). Consequently, it became of great interest to see if this abundance would be consistent with Voyager observations. Occultation measurements with the Voyager 2 radio science subsystem (RSS) [*Tyler et al.*, 1989; *Lindal et al.*, 1990] and thermal emission measurements with the infrared interferometer spectrometer (IRIS) [*Conrath et al.*, 1989, 1991*a*, *b*] have added greatly to our knowledge of the upper troposphere and lower stratosphere on Neptune. However, the IRIS measurements can only establish a temperature-dependent upper limit to the methane abundance in the stratosphere (6×10^{-3} for a temperature 155 K near 0.1 mbar) (B. Bézard, personal communication, 1991), while the RSS-derived estimate of 1–2% pertains to pressures $\gtrsim$ 1.7 bars [*Lindal et al.*, 1990].

Absorptive EUV occultations can be a powerful means of probing stratospheric structure and composition [*Smith and Hunten*, 1990; *Bishop et al.*, 1990]. During the Voyager 2 encounter with the Neptune system (closest approach occurred on August 25, 1989), both ingress and egress occultations of the Sun by Neptune were recorded with the ultraviolet spectrometer (UVS) [*Broadfoot et al.*, 1989]. The lightcurves acquired at wavelengths longward of the H_2 Lyman-Werner band systems penetrated to, and hence contain information about, the atmosphere at stratospheric pressure levels. (In this paper, we use the term "stratosphere" to refer to the region bounded by the tropopause and the methane homopause.) This was also the case for the solar occultation observed at Uranus, and the UVS occultations clearly show that the stratospheric structures on these two planets are markedly different. At Uranus, eddy mixing was found to be weak ($K_h \lesssim 10^4$ cm^2 s^{-1}), and the UVS lightcurves at wavelengths 130–165 nm all probed the equatorial stratosphere above the CH_4 photochemical peak (where unit optical depth for methane photoabsorption at H Lyman α is

[1]Now at Computational Physics, Fairfax, Virginia.

Paper number 92JE00959.
0148-0227/92/92JE-00959$05.00

reached), with the result that the lightcurves overlapped considerably in altitude [*Bishop et al.*, 1990]. At Neptune, however, the UVS lightcurves transiting the stratosphere fall into three groups: at wavelengths $\lesssim$ 135 nm, the lightcurves exhibit half-light points in the 0.1–0.3 μbar region; those at wavelengths 135–155 nm probe progressively deeper into the stratosphere; and those at wavelengths $\gtrsim$ 155 nm exhibit half-light points at pressures $\gtrsim$ 0.1 mbar. Thus the characterization of hydrocarbon abundances over an extensive pressure range is possible with the UVS occultation data. The ingress occultation occurred at a latitude of 61°N (winter hemisphere at the time of encounter, near the arctic circle), the egress occultation at 49°S (summer hemisphere), which offers the opportunity to search for latitudinal variations.

This paper presents an analysis of the UVS occultation data at wavelengths 125–138 nm, based on the premises that methane, its photochemical products (in particular, the stable C_2 hydrocarbons acetylene, ethylene, and ethane), and H_2 Rayleigh scattering constitute the major sources of UV opacity at wavelengths longward of H Lyman α (121.6 nm), and that the source for stratospheric methane is upward transport from the troposphere. Methane is expected to be the major photochemical parent in stratospheric photochemistry on Neptune. At the cold temperatures of the upper troposphere, other candidate photochemically active tropospheric species (NH_3, H_2S) are expected to freeze out at pressures too far removed from the tropopause to materially affect stratospheric chemistry [*Atreya*, 1986]. Also, photoabsorption by methane is the most plausible source of opacity at wavelengths $\lesssim$ 135 nm, which allows for fairly unambiguous inferrals of the strength of eddy mixing above the CH_4 photochemical peak and of the methane abundance in the lower stratosphere, as discussed in later sections. Our analysis is based on lightcurve simulation, utilizing an updated one-dimensional photochemical modeling code used in pre-Voyager stratospheric modeling studies [*Romani and Atreya*, 1988, 1989]. Photochemical modeling of the UVS lightcurves at longer wavelengths is deferred to a subsequent paper: the opacity at wavelengths $\gtrsim$ 140 nm is expected to stem primarily from C_2H_2, C_2H_4, and C_2H_6 photoabsorption and H_2 Rayleigh scattering, forcing a reliance on extensive modeling to unravel the constituent contributions. By contrast, the results presented in this paper are relatively insensitive to photochemical details. In the following sections, we describe the UVS occultation data, our modeling approach focusing on the inputs to the procedure, and our attempts at replicating the UVS lightcurves. We then discuss the implications of those models that are in good accord with the data with reference to previous work.

UVS Observations

The UVS instrument and its operation are described in detail by *Broadfoot et al.* [1977] and *Broadfoot et al.* [1981], and an overview of the Neptune encounter with preliminary results is presented by *Broadfoot et al.* [1989]. During occultation, the attenuation of the solar EUV spectrum by the atmosphere is monitored as the spacecraft moves into (ingress) and out of (egress) the planet shadow by recording, at 0.32 s intervals, spectra spanning the wavelength interval 53–170 nm at a resolution of ~2.5 nm. The lightcurves $I/I_\circ$ used in the present analysis are shown in Figure 1. These are obtained by ratioing, for each individual channel, the measured intensity $I(z_i)$ at minimum tangent ray height (MTRH) z_i with a mean intensity $I_\circ$ based on measurements taken prior to the onset of absorption and corrected for the limit cycle motion (modulation of the occultation signal due to spacecraft attitude control motion). At wavelengths longward of Lyman α, the background H_2-He atmosphere is itself transparent (except for Rayleigh scattering), so that these lightcurves reveal the presence and abundance of minor molecular species.

The occultation data were averaged over 0.96 s intervals prior to analysis; in conjunction with the relevant MTRH drift speeds, the altitude resolutions for the lightcurves of Figure 1 are 9.5 km (ingress) and 12.3 km (egress) to a first approximation. The actual resolution is somewhat poorer, owing to the finite width subtended by the solar disk (~5 km for ingress, ~15 km for egress). No correction for the solar disk has been applied in this analysis, however, since these widths represent at worst a blurring of neighboring resolution elements in the lightcurves of Figure 1 with no appreciable distortion of lightcurve shape. The main difficulty in our analysis lies with the scatter evident in these lightcurves, major sources of which are measurement noise, errors arising in the ratioing procedure, and uncertainties in the correction for the scattering of solar Lyman α within the instrument. Also, the ratioing procedure is more uncertain for the egress occultation than for ingress, as can be seen by comparing the ingress and egress lightcurves of Figure 1. Both data sets as used in this analysis have been rescaled to a mean $I/I_\circ$ value of 1.0 over ~200 km of atmosphere just above the onset of absorption.

Stratospheric Modeling

The data shown in Figure 1 are too steep and are affected by noise and ratioing uncertainties to too great an extent to allow a direct retrieval of (partial) profiles using the filtering-inversion technique applied to the solar occultation data obtained at Uranus [*Bishop et al.*, 1990]; instead, the procedure of lightcurve simulation has been adopted. This introduces model dependencies that must be explored, as described in this section. The main dependencies center on the adoption of a background atmosphere model and the manner in which eddy mixing (more precisely, the eddy mixing coefficient K) is assumed to vary with atmospheric pressure or number density. Once a model of the stratosphere has been specified (i.e., altitude profiles for pressure p, temperature T, and minor species mixing ratios f), it is a straightforward matter to simulate the UVS lightcurves, taking into account the occultation geometry, the known UV photoabsorption spectra of the expected stratospheric species, and characteristics of the UVS instrument like the spectral "slit" function and the channel-wavelength offset associated with the position of the Sun in the UVS field of view. The CH_4 photoabsorption cross sections used in our modeling are from *Lee and Chiang* [1983].

Model Atmosphere

The lightcurves shown in Figure 1 probe the atmosphere in the information gap between the pressure regimes mapped by the RSS ($p \gtrsim 1$ mbar) [*Lindal et al.*, 1990] and UVS ($p \lesssim 0.03$ μbar) [*Broadfoot et al.*, 1989] occultations, the latter at wavelengths in the H_2 Lyman-Werner band systems.

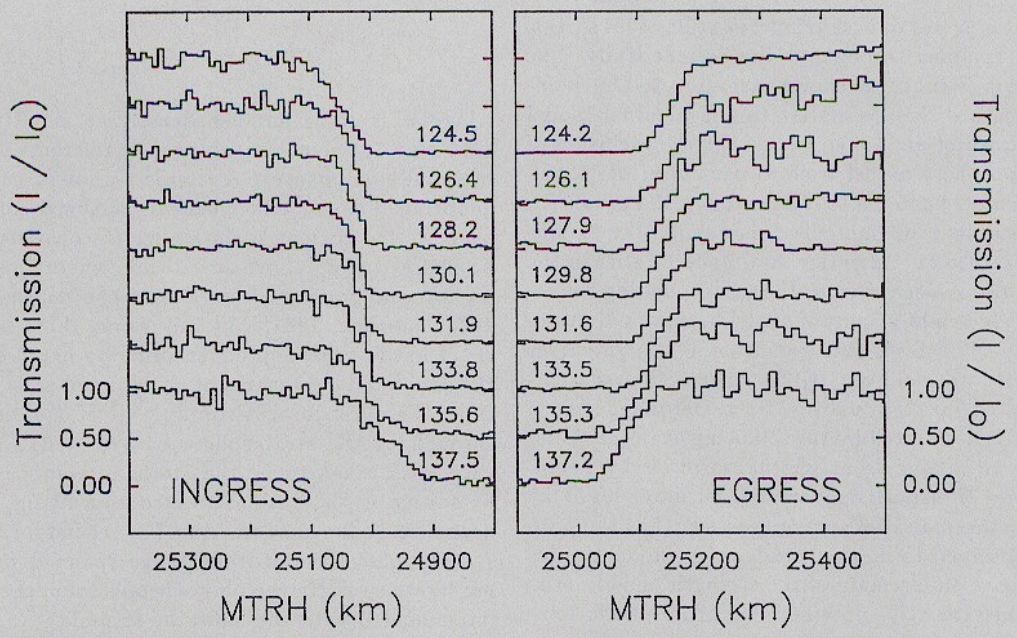

Fig. 1. Ultraviolet spectrometer (UVS) lightcurves (I/I_o versus minimum tangent ray height) used in this study, identified by channel-center wavelength. Minimum tangent ray height (MTRH) is in kilometers from planet center.

At intermediate pressures (nominally 1–30 μbar), p-T information is available from refractive stellar occultation observations [*French et al.*, 1983, 1985; *Hubbard et al.*, 1985, 1987]. The observations reported by *Hubbard et al.* [1987] are of particular interest as regards the modeling of stratospheric hydrocarbons, in that the central flash of the August 20, 1985 occultation enabled a retrieval of atmospheric temperature near the 0.4 mbar pressure level; this is near the levels of maximum contribution for the C_2H_2 and C_2H_6 IR emissions measured with the IRIS instrument [*Bézard et al.*, 1991]. We have constructed nominal p-T models for the ingress and egress latitudes using $T/T_o = (p/p_o)^\alpha$ interpolation between reference points drawn from the RSS, UVS, and stellar occultation results cited above, rescaled to a he-

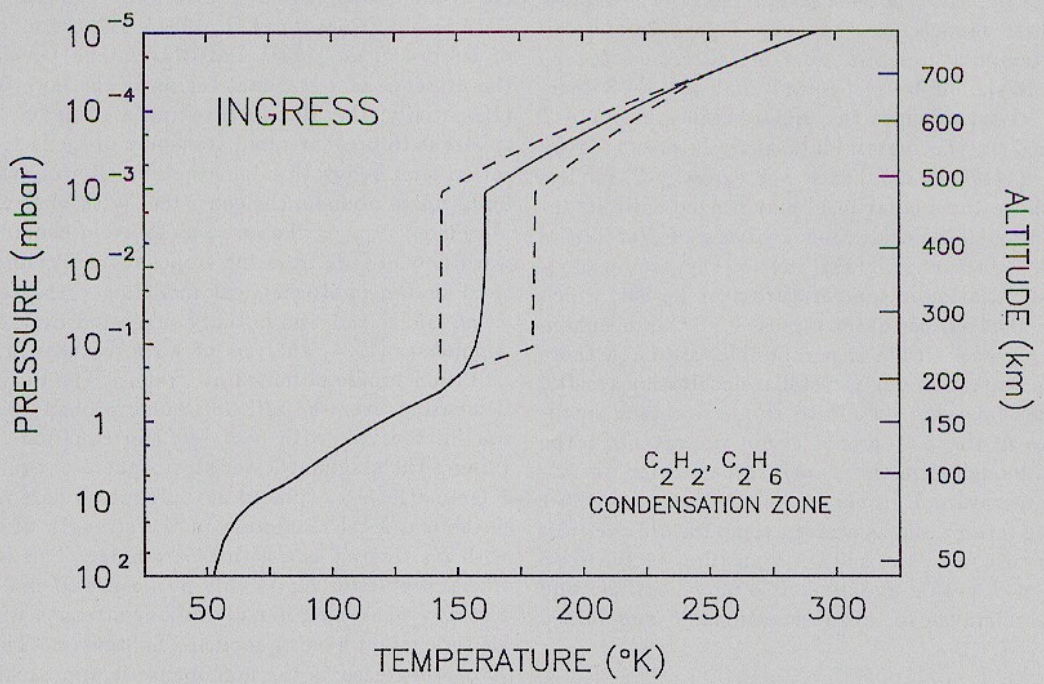

Fig. 2. Ingress stratosphere p-T models (61°N latitude). The nominal model (solid curve) has a temperature of 161 K at 1 μbar; the warm and cool models (dashed curves) have 1 μbar temperatures of 181 K and 144 K, respectively. At pressures $< 10^{-5}$ mbar, the temperature lapse rate is $dT/dz = 0.33$ K/km [*Broadfoot et al.*, 1989]. The altitude scale pertains to the nominal model, referenced to a radius of 24,445 km at the 1 bar level (see text). The egress p-T models (latitude 49°S, not shown) are very similar to the corresponding ingress models, except for the use of the egress RSS profile from *Lindal et al.* [1990] at pressures deeper than 1 mbar and the change in the planetary rotation (centrifugal) correction to gravity; the egress 1 bar radius is 24,535 km.

lium mixing ratio f(He) of 0.19 [*Conrath et al.*, 1991*a*]; this value has been assumed throughout the present study. The nominal ingress p-T model is shown in Figure 2. Our nominal p-T models are closely similar to the nominal model adopted by *Bézard et al.* [1991], except for the inclusion of the UVS thermosphere model from *Broadfoot et al.* [1989]. The 1 bar radii are 24,445 km (61°N) and 24,535 km (49°S).

Within the context of lightcurve modeling, the significance of temperature uncertainties (and uncertainties in the helium mixing ratio) derives from the corresponding uncertainty in the scale height structure of the background atmosphere. One aspect of this is that even if the UVS lightcurves could be inverted to yield a CH_4 density profile, the corresponding mixing ratios would not be model-independent. Another aspect is illustrated by the following example. Consider a lightcurve arising from photoabsorption by an inert minor species transported upward from lower levels by mixing in an isothermal atmosphere, and say that the half-light point is observed to lie at altitude $z_{1/2}$. Modeling this lightcurve will give an estimate of the strength of eddy mixing in the vicinity of $z_{1/2}$, provided the atmospheric temperature and the mixing ratio f_T of the minor species at a lower level are known. Since K is typically parameterized in terms of atmospheric number density or pressure, an underestimate (overestimate) of the atmospheric temperature will lead directly to an overestimate (underestimate) in the value of K to maintain the proper half-light altitude in the modeled lightcurve.

To explore the uncertainties associated with the specification of the background atmosphere at pressures between 1 mbar and 0.03 μbar, "warm" and "cool" p-T models have been constructed based on the range of temperatures near 1 μbar inferred from a number of stellar occultation analyses [*Hubbard et al.*, 1985; *French et al.*, 1985]. The ingress versions of these models are shown in Figure 2, and are identified by temperatures at 1 μbar of 182 K and 144 K, respectively. It should be recognized that the UVS thermosphere model that defines the upper reaches of our p-T models is based on the ingress data analysis presented by *Broadfoot et al.* [1989], and hence our egress p-T models at altitudes above the 1 μbar level may not be entirely appropriate. The stellar occultation analyses of *Hubbard et al.* [1985] and *French et al.* [1985] do not suggest an obvious latitudinal variation in temperature near 1 μbar, which might indicate that our use of the ingress UVS thermosphere model at the egress latitude is permissible, although there is considerable scatter among the stellar occultation results. (Note: It is perhaps worthwhile to emphasize that small-scale structure in the p-T profile is not important in the context of the modeling in this paper; in particular, the atmospheric temperature T in our models at pressures 100-1 μbar should be interpreted as a mean temperature over this pressure interval. Also, the sudden transition to the UVS thermosphere p-T profile at 1 μbar is a model artifact and should not be mistaken for an observationally constrained feature.)

Eddy Mixing Profiles

In one-dimensional stratospheric-mesospheric modeling it has been conventional to adopt for the eddy mixing coefficient K a dependence on an inverse power of the background number density

$$K(z) = K_o \times \left(\frac{n_o}{n(z)}\right)^{\beta} \qquad (1)$$

where n is total number density, z is altitude, and the subscript "o" denotes values at a reference level (e.g., the methane homopause). A simple argument can be made for adopting $\beta \approx 1/2$ under certain idealized conditions, while over limited regions maintaining K constant ($\beta = 0$) may be justified (e.g., above an altitude where upward propagating internal gravity waves "break") [*Lindzen*, 1971; *Hunten*, 1975; *Lindzen*, 1981]. In this work, three basic forms for $K(z)$ have been adopted, in order to explore the effect on the simulated lightcurves of an assumed eddy mixing profile type. The first form is simply that of equation (1) applied throughout the stratosphere with $\beta = 1/2$ and the reference level taken to be the methane homopause (indicated by subscript "h"); K_h is treated as a fitting parameter, as described in the next section. The second form has constant K throughout the altitude range spanned by the 125–138 nm lightcurves. In the photochemical models, this form was implemented with the following formula

$$\begin{aligned} K &= K_1, \quad (p \geq p_1) \\ &= K_1 \times \left(\frac{p}{p_1}\right)^{\gamma}, \quad (p_1 > p > p_2) \\ &= K_2, \quad (p \leq p_2) \end{aligned} \qquad (2)$$

where $\gamma = \ln(K_2/K_1)/\ln(p_2/p_1)$. The value of K_2 is obtained from UVS comparisons. This form has a stagnant layer ($K_1 \approx 2 \times 10^3$ cm^2 s^{-1}) in the lower stratosphere ($p_1 \approx$ 1 mbar), in line with an estimate for the rate of overturning of the atmosphere at pressures deeper than 1 mbar from IRIS results [*Conrath et al.*, 1991*b*] and the modeling results of *Bézard et al.* [1991] and *Moses* [1991] which argue for the presence of a stagnant region in the lower stratosphere. (Essentially, the idea in invoking a stagnant lower stratosphere is to prevent rapid transport of C_2H_6 to the condensation sink below 10 mbar, thereby allowing this species to build up to abundances consistent with observations.) The placement of p_1 is chosen so as to avoid choking off the upward flow of CH_4 from the troposphere. A similar form was used in the photochemical modeling presented by *Bézard et al.* [1991] and was initially suggested by the *Hinson and Magalhães* [1991] analysis of wave features in the RSS occultation profile obtained at Uranus. The third form has K decreasing over the altitude range probed by the 125–138 nm lightcurves, with $\beta = -1/2$ in equation (1), while retaining the stagnant lower stratosphere of equation (2); the reference level p_o (placed at 0.01 mbar) here refers to a hypothetical local maximum in the strength of eddy mixing, with K_o treated as a fitting parameter. This is a highly artificial profile for K; its only purpose is to explore the effect a steady weakening in eddy mixing strength with increasing altitude might have on modeled lightcurves. The notion that K can decrease as the homopause is approached is in itself not implausible, however, as argued by *Lindzen* [1981]. It is important to keep in mind that in the comparisons with the UVS data described in the next section, only the value of the eddy mixing coefficient in the vicinity of the lightcurve half-light altitudes ($K_{1/2}$) is physically significant; at deeper levels, the only constraint on K is that eddy mixing must

remain strong enough to avoid stifling the upward flux of CH_4 from the troposphere.

Lyman α Fluxes and Photochemistry

The distribution of methane in our steady-state one-dimensional models is basically governed by upward transport from the tropopause to a level above which loss via photolysis occurs. A reference altitude for this level can be identified as that altitude at which unit optical depth for photoabsorption by CH_4 at Lyman α is reached, since photons at this wavelength are effective in dissociating CH_4 and the flux at this wavelength dominates the solar EUV irradiance spectrum. A solar maximum irradiance spectrum (with a line-integrated Lyman α flux of 5×10^{11} cm^{-2} s^{-1} at 1.0 AU) has been used in the current modeling, incident at mean solar zenith angles of 88° and 50° for ingress and egress modeling, respectively, with diurnal averaging. *Strobel et al.* [1990] have pointed out, in a study of methane photochemistry on Triton, that the Lyman α flux from the local interstellar medium (LISM) leads to a CH_4 photodissociation rate comparable to solar rates at Neptune's distance from the Sun. The LISM contribution has been included in the current modeling as a flux of 1.6×10^8 cm^{-2} s^{-1} incident at a zenith angle of 50°; this is a sky-averaged value based on LISM Lyman α measurements acquired with the UVS instrument near encounter. The LISM Lyman α flux is the principal driver of CH_4 photochemistry at the near-arctic latitude of the ingress occultation. The net lifetime against Lyman α photodissociation at 61°N is 4.5×10^8 s (LISM and solar illumination combined), while at egress it is 1.2×10^8 s; these are short compared with the length of the Neptune year (5.2×10^9 s), justifying the use in our modeling of illumination angle values pertaining to the occultation latitudes at the time of encounter.

The photochemical modeling code used to determine the methane mixing ratio profile consistent with the above inputs is based on a one-dimensional steady-state scheme that has been described previously [*Romani and Atreya*, 1988, 1989]. It incorporates vertical mixing via molecular diffusion and eddy mixing, and handles self-consistently the condensation of C_2H_2, C_2H_6, and C_4H_2 to their respective ices. A listing of the reactions currently included in the model is given by *Bézard et al.* [1991]. The full code has been used in the current modeling, both to account for the recycling of CH_4 following photodissociation and to estimate the relatively minor contribution to the opacity at wavelengths 125–138 nm arising from the stable C_2 hydrocarbons. For all models explored in this study, methane itself is the major source of opacity at these wavelengths (as illustrated below). The CH_4 recycling fraction, defined as the ratio of the column-summed chemical production rate of CH_4 above the tropopause (predominately via $CH_3 + H + M \rightarrow CH_4 + M$) to the column-summed photodissociation rate, is in the range 0.40–0.55 for the ingress models discussed below and 0.30–0.35 for the egress models.

DATA-MODEL COMPARISONS

The simulation of the 125–138 nm lightcurves has been carried out by treating the value of the eddy mixing coefficient in the region of the half-light altitudes ($K_{1/2}$) and the methane mixing ratio in the lower stratosphere ($f_T(CH_4)$) as fitting parameters, for each combination of prescribed inputs (e.g., p-T model and assumed eddy mixing profile form). The procedure has been to fix one parameter ($f_T(CH_4)$) and vary the other ($K_{1/2}$, via K_o in equation (1) or K_2 in equation (2)) until the model lightcurves at wavelengths $\lesssim$ 130 nm exhibit the correct mean half-light altitude: for a prescribed value for either one of the fitting parameters, increasing the value of the other shifts the half-light points of the model lightcurves to higher altitudes. Once this step has been carried out for a range of prescribed $f_T(CH_4)$ values, the degree to which the model lightcurves corresponding to a $(f_T(CH_4), K_{1/2})$ pair replicate the spacing and steepness of the UVS lightcurves over the 125–138 nm interval can be used to assess whether a model is acceptable or not. This allows us to take full advantage of the contiguous set of UVS lightcurves at wavelengths over which the methane photoabsorption cross section begins to decrease with increasing wavelength. Acceptable models are characterized by fairly narrow ranges in $f_T(CH_4)$ and $K_{1/2}$ (generally less than a factor of 2, with the constraint that an increase in one parameter must be accompanied by a decrease in the other to preserve an acceptable fit.)

The noise and ratioing uncertainties in the UVS data preclude an unambiguous implementation of this procedure, leaving one to choose whether to give greater relative weight to lightcurve spacing or to shape (steepness). Throughout, the comparison of model lightcurves with UVS data has been done visually. To compensate for this, we prefer to give greater weight to lightcurve spacing. The least ambiguous manifestation of this is in the spacing between MTRHs where the various lightcurves go black; this is also the criterion least compromised by uncertainties in the correction for Lyman α scattering within the instrument. In Figure 3*a*, we show ingress UVS lightcurves compared with model lightcurves judged to be acceptable using this criterion. The corresponding methane mixing ratio and eddy mixing profiles are shown in Figure 3*b*. The nominal p-T atmosphere has been used in these models, hence these will be referred to as our standard ingress models: model "a" for K increasing in inverse proportion to the square root of the atmospheric number density and model "b" for K constant above ~0.1 mbar. It is evident that either of these models gives a good fit to the data, with agreement on the value of $f_T(CH_4)$ to within modeling uncertainties (specifically, the uncertainties associated with making visual judgments of model fits).

Also shown in Figure 3*b* are models in which the methane mixing ratio in the lower stratosphere has been held to a typical saturation-limited ("cold trap") value (3×10^{-5}; models "s"), based on the cold tropopause temperatures revealed by the Voyager RSS occultations [*Lindal et al.*, 1990], and models in which methane is present in amounts suggested by analyses of pre-Voyager ground-based IR brightness measurements (3×10^{-3}; models "h") [*Orton et al.*, 1987, 1990; *Bézard et al.*, 1991]. The strength of eddy mixing ($K_{1/2}$) in these models was varied to try to yield the correct placement of the half-light points over the 125–138 nm wavelength interval; the most successful attempts are shown in Figure 3*c*. It can be seen that the saturation-limited lightcurves (dashed curves) are not steep enough and are too widely spaced to be consistent with the UVS data over the 125–138 nm wavelength interval; the models suggested by the ground-based IR analyses (models "h," solid curves), on the other hand, are too steep and too closely spaced. In Table 1, values of various parameters characterizing the mod-

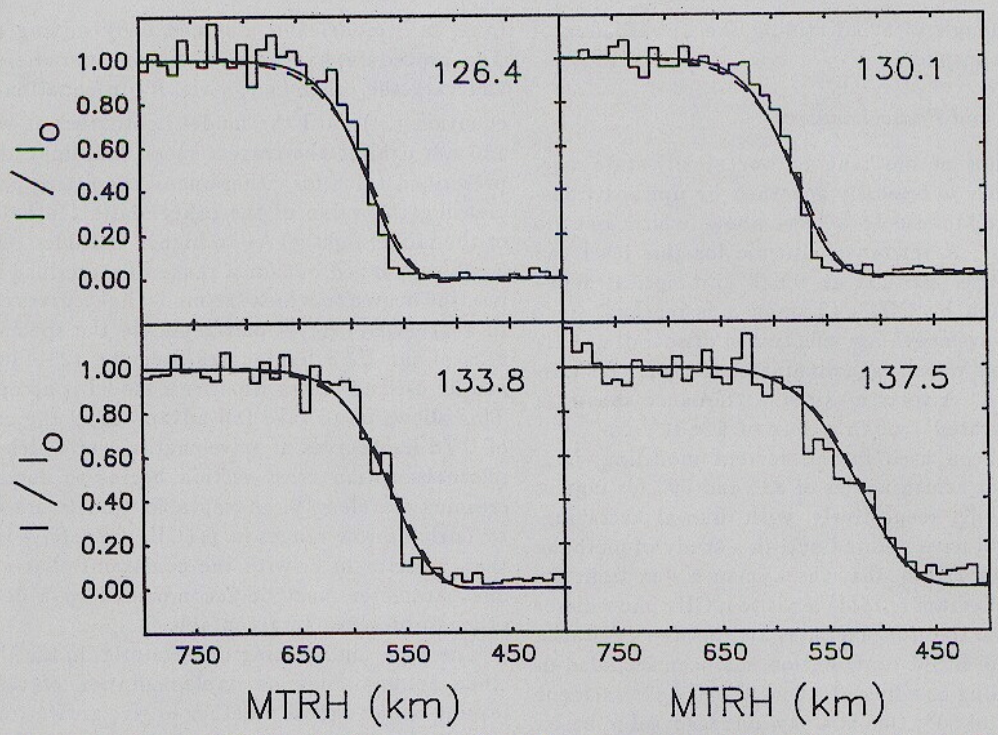

Fig. 3*a*. Comparison of UVS ingress lightcurves (identified by channel-center wavelength) with model lightcurves giving good overall agreement with the data (i.e., the standard ingress models described in the text). The models are characterized by the type of eddy mixing profile adopted in the modeling: K increasing in inverse proportion to the square root of the background number density (dashed curves, model "a" in Figure 3*b*) and K held constant throughout the altitude range probed by these lightcurves (solid curves, model "b" in Figure 3*b*). In this and the following figures, MTRH is referenced to the 1 bar level.

els shown in Figure 3 are given; the $\tau = 1$ entries refer to the CH_4 photodissociation peak, here evaluated along a 50° slant angle (i.e., the slant angle used for the incident LISM Lyman α flux and solar EUV flux at egress).

In Figure 4, the constituent opacities entering into the model "b" lightcurves at channel-center wavelengths 126.4 nm and 137.5 nm are shown, illustrating that photoabsorption by methane is the major source of opacity in these models at the wavelengths of interest. The contribution from H_2 Rayleigh scattering is quite negligible, and the summed

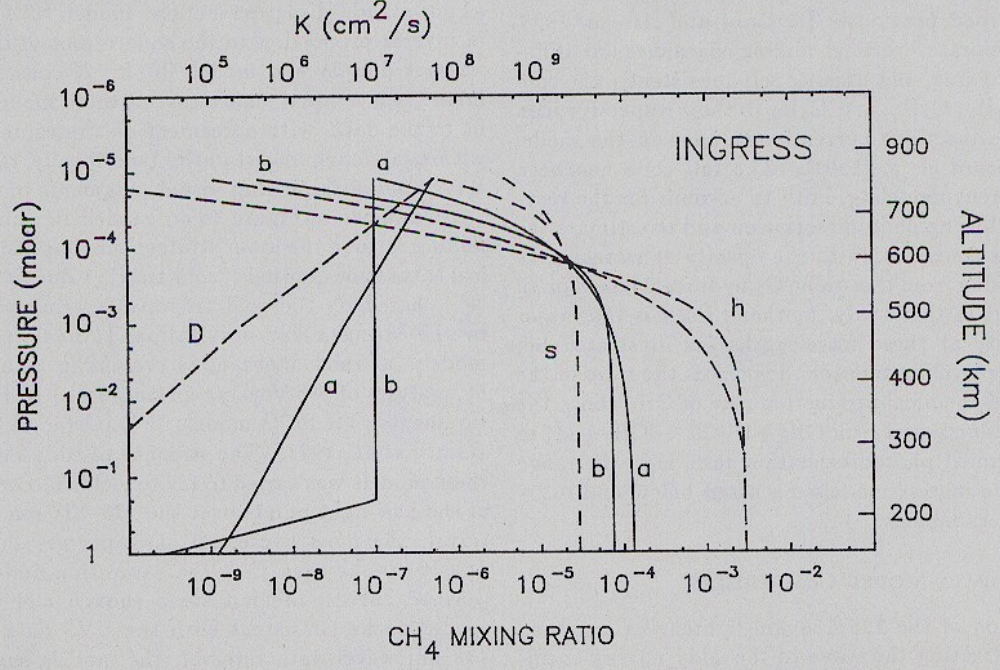

Fig. 3*b*. Methane mixing ratio profiles for our standard ingress models (models "a" and "b"), for models wherein the methane abundance in the lower stratosphere is limited by "cold trap" saturation (models "s"), and for models wherein the abundance adopted by *Bézard et al.* [1991] is assumed (models "h"). Also shown are the eddy mixing profiles belonging to the standard ingress models. See Table 1 for parameter values.

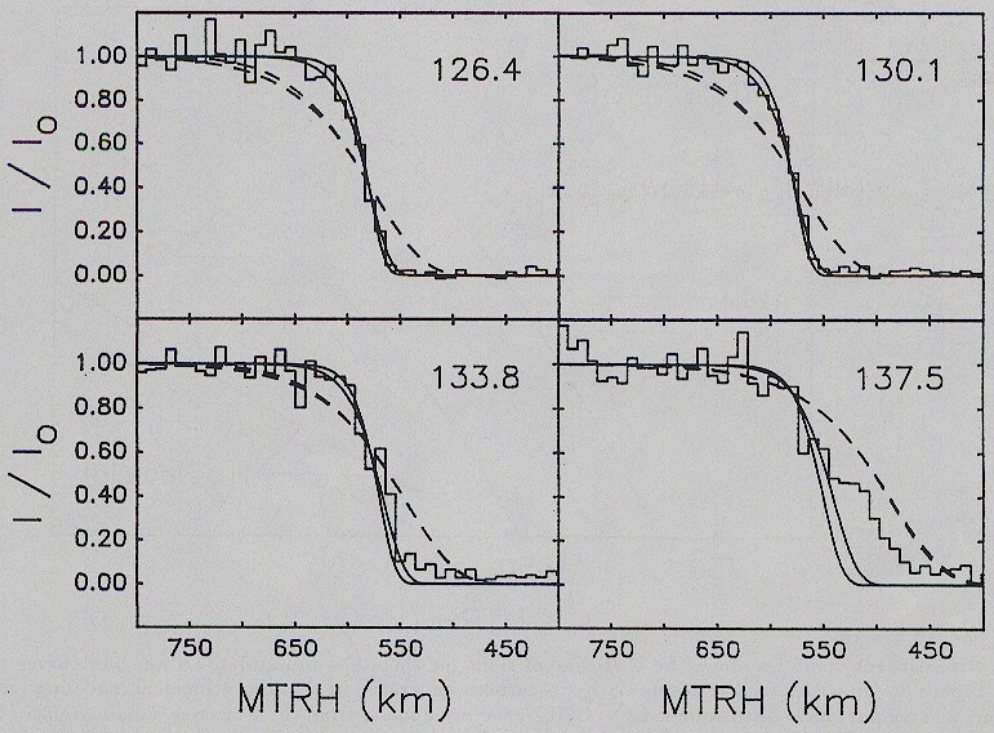

Fig. 3c. Comparison of UVS ingress lightcurves with model lightcurves in which the methane mixing ratio in the lower stratosphere takes on prescribed values: $f_T(CH_4) = 3 \times 10^{-3}$ (solid curves, models "h" in Figure 3b) and $f_T(CH_4) = 3 \times 10^{-5}$ (dashed curves, models "s" in Figure 3b). Two models are illustrated for each specified value of $f_T(CH_4)$: K held constant and K increasing with decreasing pressure (see equation (1)).

contribution from the stable C_2 hydrocarbons (acetylene, ethylene, ethane) is also minor. The main C_2 contributor at 137.5 nm in both standard ingress photochemical models is C_2H_4.

As noted earlier, there is some ambiguity in specifying a criterion by which the acceptability of a set of simulated lightcurves can be judged. In Figures 5a-5c, we show models that might be considered acceptable on the basis of the fit to the shape of the lightcurves at wavelengths $\lesssim$ 130 nm; models "A" and "B" are analogous to models "a" and "b" of Figure 3, respectively, while model "C" incorporates the form for the K profile with $\beta = -1/2$. The lightcurves from the models incorporating the nominal p-T atmosphere are shown in Figure 5a. There is a distinct problem with these fits, in that all of these models are too opaque at the 138 nm channel. In general, to fit the steep shapes apparent in the UVS lightcurves, a combination of larger $f_T(CH_4)$ and smaller $K_{1/2}$ is needed compared with the standard models, which in turn causes a reduction in the MTRH spacing of the lightcurves at wavelengths $\gtrsim$ 130 nm. This may be taken as a further indication that the spacing criterion used for the models of Figure 3 is more appropriate.

The different imposed forms for the K profile in models "A" and "B" lead to a range in $f_T(CH_4)$ values larger than arises in the models of Figure 3 (and larger than the uncertainty stemming from the reliance on visual judgments). By contrast, the variation in $f_T(CH_4)$ in switching from $\beta = 0$ (model "B") to $\beta < 0$ (model "C") in the K profile is small enough to be insignificant. This is also the case when the spacing criterion of Figure 3 is employed in conjunction with $\beta = 0$ versus $\beta < 0$ K profiles. If we had an independent way of determining $f_T(CH_4)$ and if there was not a problem in the fits at the longer wavelengths, then our ingress models indicate that the $\lesssim$ 130 nm lightcurves might hold the possibility of inferring the form of the K profile near the half-light levels, but only if $\beta > 0$. However, it does not seem

TABLE 1. Ingress Models

Label in Figures	β	$f_T(CH_4)$	$z_{\tau=1}$, km	$K_{\tau=1}$, $cm^2 s^{-1}$	$f(CH_4)_{\tau=1}$	$K^{\dagger}_{1/2}$, $cm^2 s^{-1}$	$f(CH_4)^{\dagger}_{1/2}$	z_h, km	p_h, mbar	K_h, $cm^2 s^{-1}$
a	1/2	1.3×10^{-4}	442	2.8×10^6	8.4×10^{-5}	1.0×10^7	2.9×10^{-5}	803	1.3×10^{-5}	5.0×10^7
b	0	7.4×10^{-5}	439	10^7	6.9×10^{-5}	10^7	3.4×10^{-5}	678	4.9×10^{-5}	10^7
A	1/2	8.8×10^{-4}	478	1.7×10^6	2.4×10^{-4}	4.3×10^6	3.8×10^{-5}	678	4.9×10^{-5}	10^7
B	0	1.3×10^{-4}	458	6.0×10^6	1.1×10^{-4}	6.0×10^6	3.9×10^{-5}	647	7.5×10^{-5}	6.0×10^6
BWARM	0	9.9×10^{-5}	459	3.0×10^6	7.7×10^{-5}	3.0×10^6	2.2×10^{-5}	644	1.4×10^{-4}	3.0×10^6
BCOOL	0	3.4×10^{-4}	468	9.0×10^6	2.8×10^{-4}	9.0×10^6	8.0×10^{-5}	632	5.2×10^{-5}	9.0×10^6
C	−1/2	1.0×10^{-4}	453	1.6×10^7	9.6×10^{-5}	5.3×10^6	3.9×10^{-5}	620	1.1×10^{-4}	3.8×10^6
h	0	3.0×10^{-3}	511	1.4×10^6	6.7×10^{-4}	1.4×10^6	6.0×10^{-5}	567	2.5×10^{-4}	1.4×10^6
h	1/2	3.0×10^{-3}	494	1.3×10^6	4.0×10^{-4}	2.9×10^6	4.6×10^{-5}	637	8.6×10^{-5}	5.0×10^6
s	0	3.0×10^{-5}	400	5.0×10^7	2.8×10^{-5}	5.0×10^7	2.4×10^{-5}	803	1.3×10^{-5}	5.0×10^7
s	1/2	3.0×10^{-5}	405	8.1×10^6	3.0×10^{-5}	4.3×10^7	2.3×10^{-5}	1070	1.6×10^{-6}	7.0×10^8

†Evaluated at 575 km altitude ($p = 2.2 \times 10^{-4}$ mbar, nominal model).

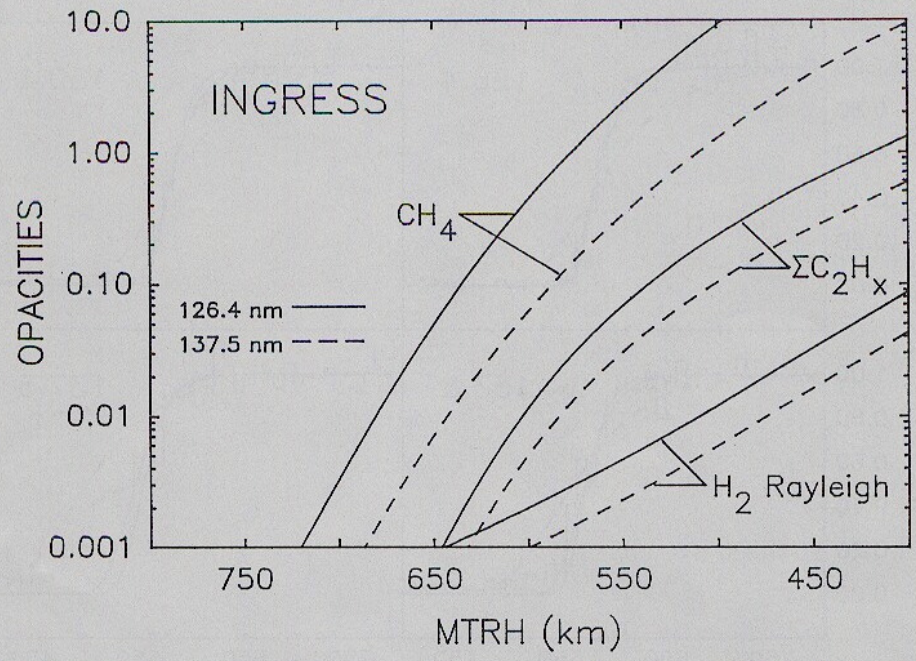

Fig. 4. Constituent opacities along the UVS line of sight for the 126.4 nm and 137.5 nm lightcurves of model "b" in Figure 3. Opacities for the stable C_2 hydrocarbons generated in the photochemical modeling (acetylene, ethylene, and ethane) have been summed ($\sum C_2H_x$); the net opacity from these species remains relatively minor compared with the CH_4 opacity even at the longer wavelength.

possible to extract reliable estimates of all three quantities ($f_T(CH_4)$, $K_{1/2}$, and β) using the UVS lightcurves alone.

In Figure 5c, examples of acceptable fits (at $\lesssim$ 130 nm) using the steepness criterion with the "cool" and "warm" background atmospheres are shown; $f_T(CH_4)$ and $K_{1/2}$ values each shift by a factor $\sim$2 downward (upward) for the warm (cool) atmosphere model, since the half-light altitudes now correspond to a deeper (shallower) pressure level. Shifts of the same magnitude occur for models conforming to the spacing criterion of Figure 3. The implications of these mod-

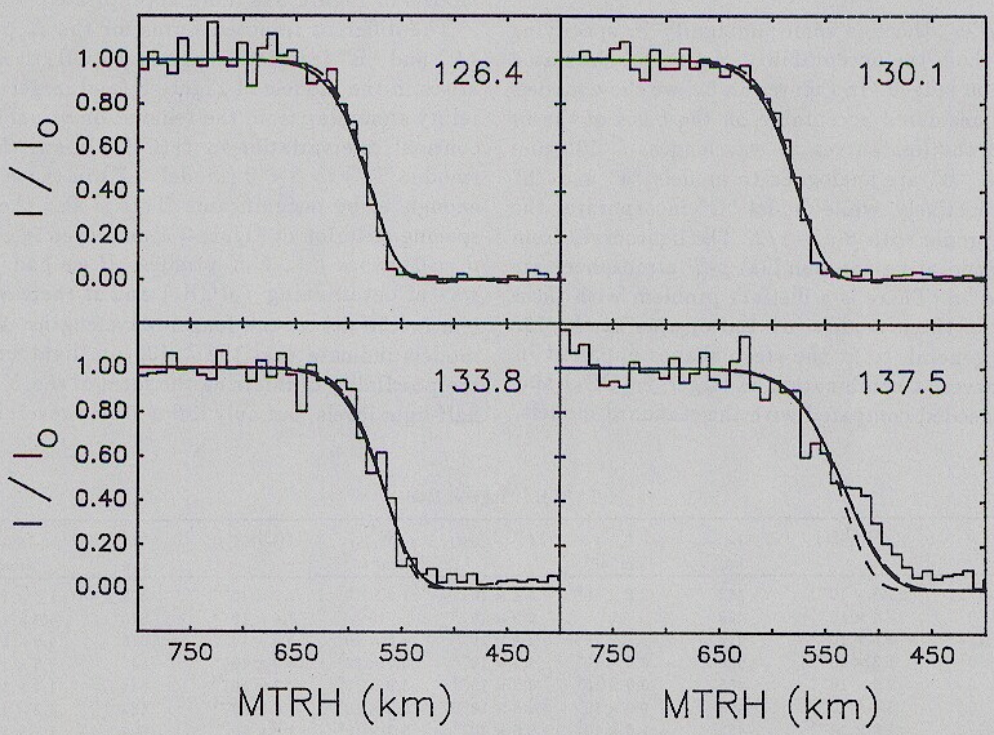

Fig. 5*a*. Model lightcurves giving good agreement with the ingress UVS data at wavelengths $\lesssim$ 130 nm for three eddy mixing profile types: K increasing in inverse proportion to the square root of the background number density (dashed curves, model "A" in Figure 5*b*), K decreasing in proportion to the square root of the background number density (longer-dashed curves, model "C" in Figure 5*b*), and K held constant throughout the altitude range probed by these lightcurves (solid curves, model "B" in Figure 5*b*).

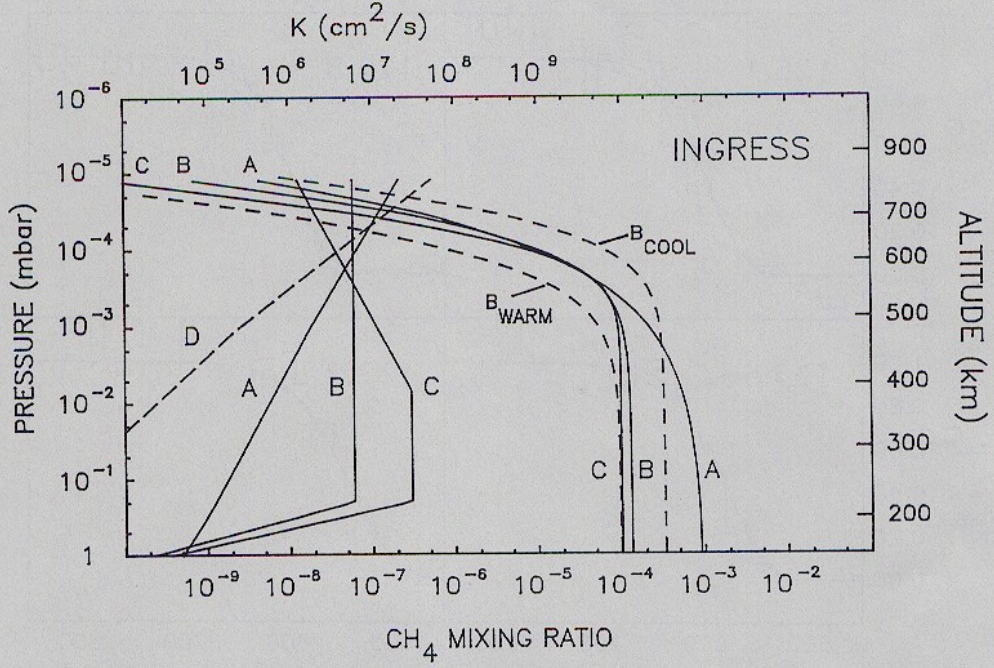

Fig. 5*b*. Methane mixing ratio profiles for models illustrating the sensitivity of the lightcurve simulation procedure to changes in the manner in which the strength of eddy mixing is assumed to vary with altitude (models "A," "B," and "C," all incorporating the nominal p-T model) and to uncertainties in the ingress p-T profile (models "B_{WARM}" and "B_{COOL}"). Also shown are the eddy mixing profiles belonging to the "A," "B," and "C" models. See Table 1 for parameter values. (The altitude scale pertains to the nominal p-T model.)

els are discussed below. Various parameter values for the models shown in Figure 5 are included in Table 1.

Egress versions of the models of Figure 3 (i.e., our standard egress models) are shown in Figure 6, along with models exhibiting saturation-limited versus IR-derived $f_T(CH_4)$ values. The models replicating the egress UVS data are consistent with those of the ingress analysis, with an increase in $K_{1/2}$ by a factor $\sim$2 throughout. As stated earlier, the egress data are subject to greater ratioing uncertainties than the ingress data (as evidenced by the 126.1 nm lightcurve in Figure 6), and consequently more ambiguity attends the identification of a good fit. It might be that the slightly

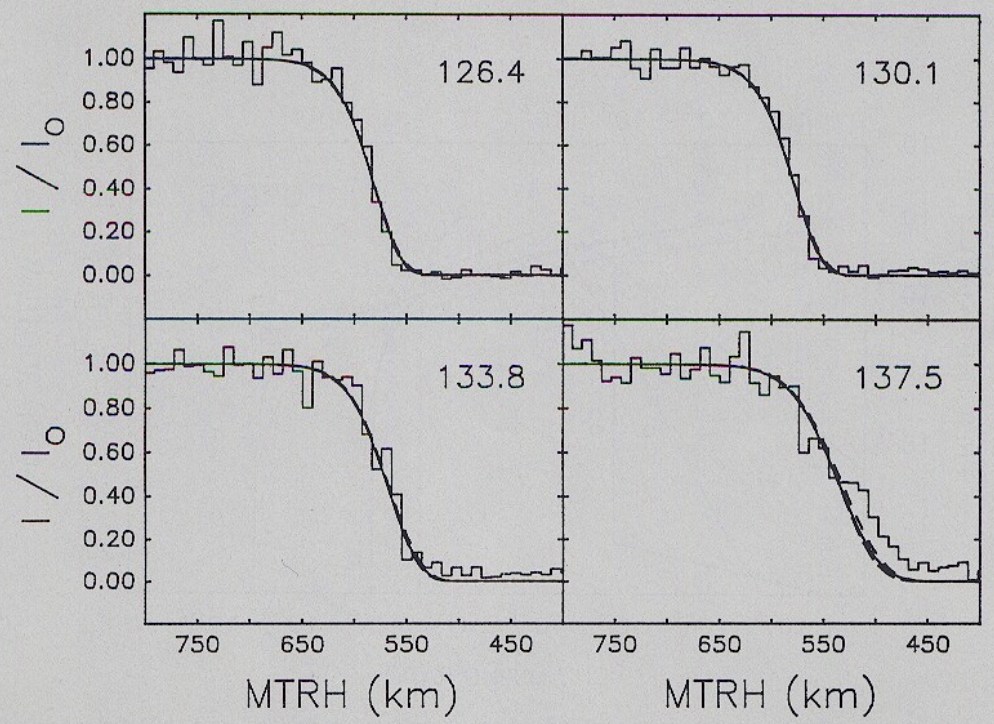

Fig. 5*c*. Model lightcurves giving good agreement with the ingress UVS lightcurves at wavelengths $\lesssim$ 130 nm for the p-T models of Figure 2: nominal (solid curve, "B" in Figure 5*b*), warm (longer-dashed curve, "B_{WARM}" in Figure 5*b*), and cool (dashed curve, "B_{COOL}" in Figure 5*b*).

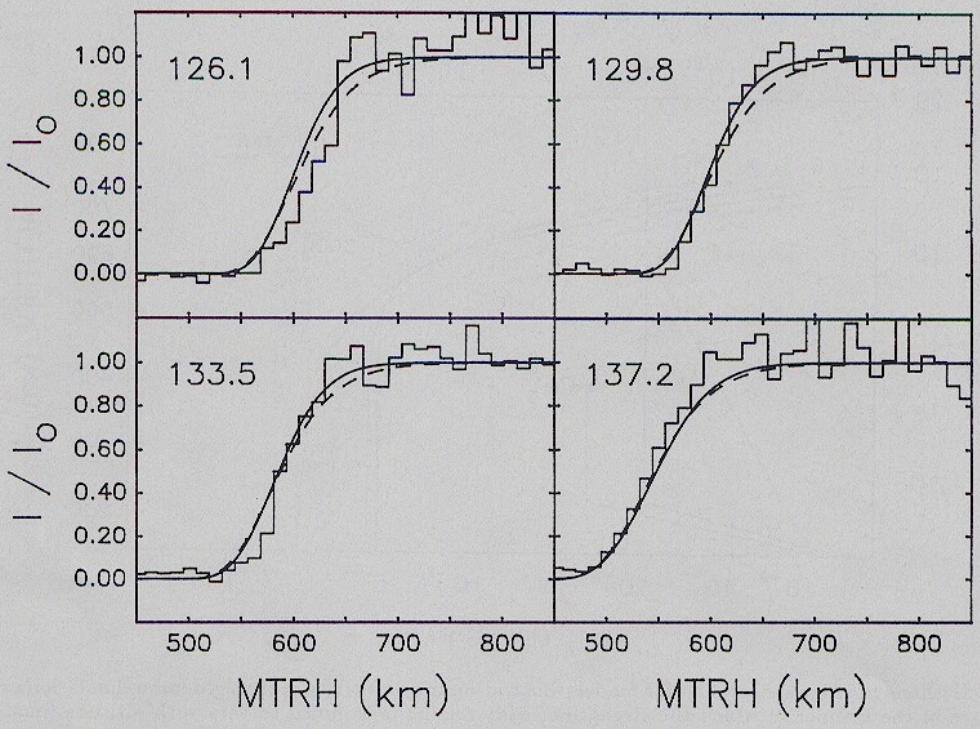

Fig. 6*a*. Comparison of UVS egress lightcurves (identified by channel-center wavelength) with model lightcurves giving good overall agreement with the data (i.e., the standard egress models "a" and "b" of Figure 6*b*). Refer to the legend of Figure 3*a*.

larger $K_{1/2}$ values of the egress fits arise in part from the use of the ingress UVS thermosphere profile in our egress p-T models. Nevertheless, sensitivities to the assumed form of the K profile and background p-T model are very similar to the ingress cases discussed above, and the inferred $f_T(CH_4)$ values are in satisfying accord with the ingress modeling results. Parameter values are given in Table 2 for the models of Figure 6 and for models (not shown) paralleling the ingress models of Figure 5.

DISCUSSION

The data-model comparisons of the previous section demonstrate that, given a background p-T model, the 125–138 nm lightcurves serve to delineate fairly narrow ranges

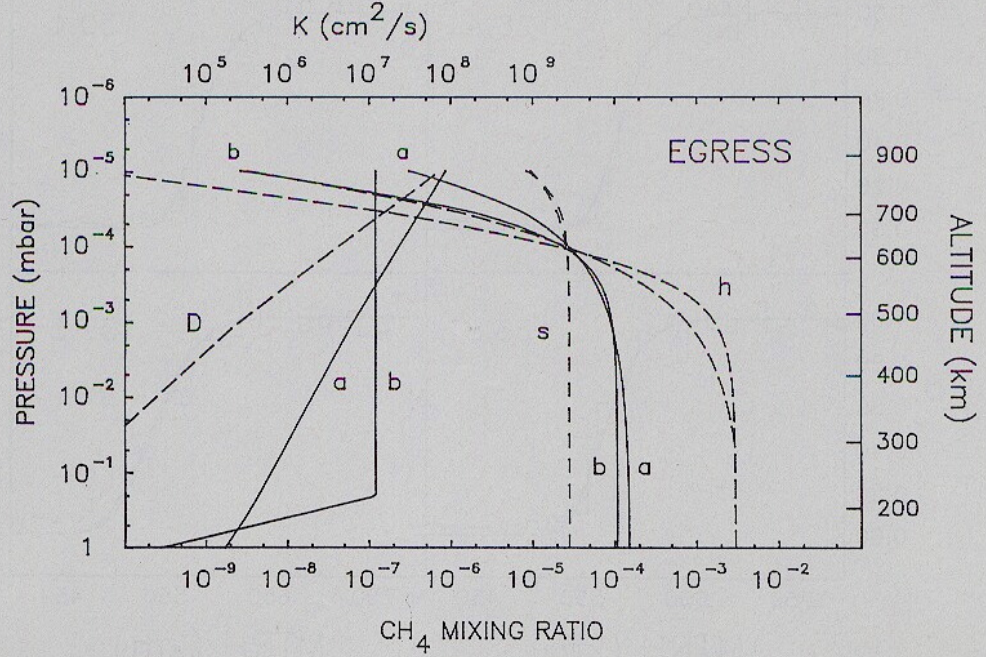

Fig. 6*b*. Methane mixing ratio profiles for our standard egress models (models "a" and "b"), for models wherein the methane abundance in the lower stratosphere is limited by cold trap saturation (models "s"), and for models wherein the abundance adopted by *Bézard et al.* [1991] is assumed (models "h"). Also shown are the eddy mixing profiles belonging to the standard egress models. See Table 2 for parameter values.

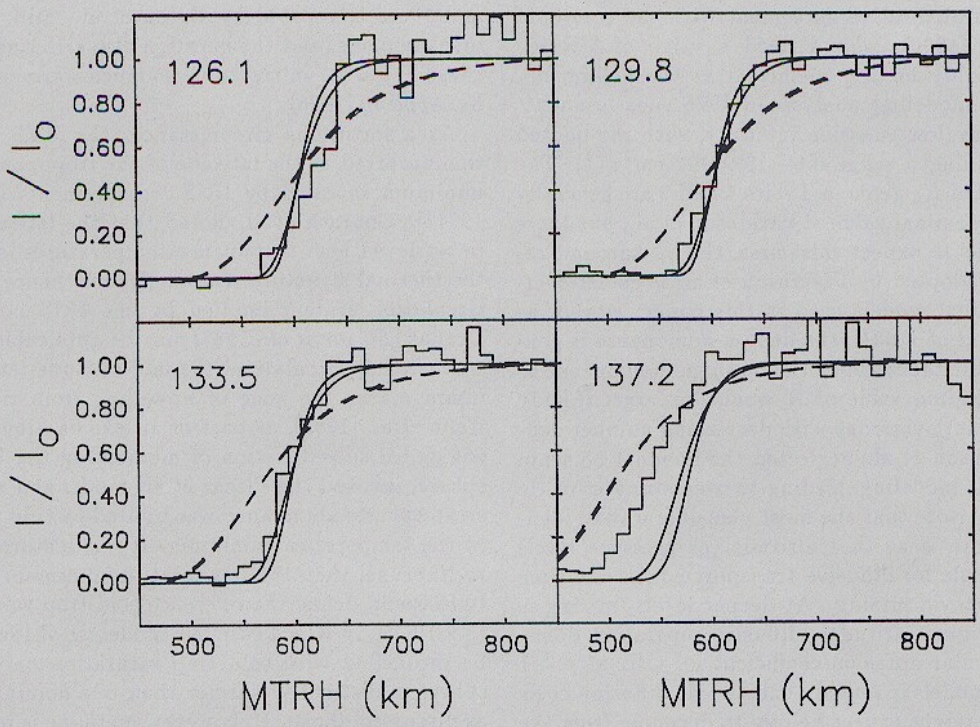

Fig. 6c. Comparison of UVS egress lightcurves with model lightcurves in which the methane mixing ratio in the lower stratosphere takes on prescribed values (refer to the legend of Figure 3c).

in both the value of the eddy mixing coefficient $K_{1/2}$ above the methane photolysis peak and compatible methane mixing ratios $f_T(CH_4)$ in the lower stratosphere, the former corresponding to the region where these lightcurves exhibit their half-light points. If the nominal p-T models adopted in this study are appropriate, then a $K_{1/2}$ value of $\sim 10^7$ $cm^2\ s^{-1}$ near 0.2 μbar for the ingress occultation is indicated (slightly larger values holding for egress), with $f_T(CH_4)$ in the range $7-20 \times 10^{-5}$. On the one hand, use of a larger value of $f_T(CH_4)$ ($\gtrsim 10^{-3}$) in the modeling requires a reduction in $K_{1/2}$ to obtain the correct mean half-light altitude for the $\lesssim 130$ nm lightcurves, but the modeled lightcurves at the longer wavelengths are then too opaque compared with the UVS data. On the other hand, use of a smaller value of $f_T(CH_4)$ ($\sim 3 \times 10^{-5}$) forces an increase in $K_{1/2}$ with a concomitant decrease in steepness and increase in MTRH spacing in the model lightcurves to the extent that these models can also be disqualified.

However, our nominal p-T models may not be appropriate, and the uncertainties in atmospheric p-T structure have been explored (see Figures 2 and 5). Use of a cooler p-T model forces increases in both $f_T(CH_4)$ and $K_{1/2}$ to obtain acceptable model lightcurves; however, $f_T(CH_4) < 10^{-3}$ is still indicated. If the mean temperature at pressures 100–1 μbar is considerably warmer ($T \gtrsim 170$ K) than in our nominal models (155–160 K), then values of $f_T(CH_4)$ compatible with saturation at the tropopause are admitted. In fact, the "cold trap" value for $f_T(CH_4)$ for the nominal ingress p-T model of Figure 2 is 6×10^{-5} (established at the tropopause with temperature 52.3 K at 135 mbar). This is quite close to the $f_T(CH_4)$ value of model "b" in Figure 3 and Table 1, so that it can be argued that the ingress data are consistent with saturation $f_T(CH_4)$ values, without having to invoke warmer temperatures. The cold trap value for the egress p-T models is 3×10^{-5} (established at an altitude ~ 8 km below the nominal tropopause with temperature 50.8 K at 135 mbar). This value for $f_T(CH_4)$ is not consistent with the egress data (as shown in Figure 6), unless a distinctly warmer stratosphere is present.

The strength of eddy mixing inferred from our data-model

TABLE 2. Egress Models

Label in Figures	β	$f_T(CH_4)$	$z_{\tau=1}$, km	$K_{\tau=1}$, $cm^2\ s^{-1}$	$f(CH_4)_{\tau=1}$	$K^{\dagger}_{1/2}$, $cm^2\ s^{-1}$	$f(CH_4)^{\dagger}_{1/2}$	z_h, km	p_h, mbar	K_h, $cm^2\ s^{-1}$
a	1/2	1.5×10^{-4}	452	4.6×10^6	1.0×10^{-4}	1.8×10^7	3.8×10^{-5}	871	7.6×10^{-6}	10^8
b	0	1.1×10^{-4}	454	1.2×10^7	9.8×10^{-5}	1.2×10^7	3.9×10^{-5}	691	4.2×10^{-5}	1.2×10^7
A	1/2	7.9×10^{-4}	487	2.7×10^6	2.7×10^{-4}	7.8×10^6	4.7×10^{-5}	727	2.8×10^{-5}	2.0×10^7
B	0	1.7×10^{-4}	470	10^7	1.5×10^{-4}	10^7	5.1×10^{-5}	679	4.9×10^{-5}	10^7
BWARM	0	8.2×10^{-5}	457	6.0×10^6	7.0×10^{-5}	6.0×10^6	2.4×10^{-5}	688	7.7×10^{-5}	6.0×10^6
BCOOL	0	3.4×10^{-4}	475	1.8×10^7	3.0×10^{-4}	1.8×10^7	1.1×10^{-4}	676	3.1×10^{-5}	1.8×10^7
C	−1/2	1.3×10^{-4}	466	2.7×10^7	1.2×10^{-4}	8.8×10^6	5.2×10^{-5}	649	7.3×10^{-5}	6.2×10^6
h	0	3.0×10^{-3}	527	2.4×10^6	8.5×10^{-4}	2.4×10^6	7.9×10^{-5}	595	1.6×10^{-4}	2.4×10^6
h	1/2	3.0×10^{-3}	509	2.2×10^6	5.2×10^{-4}	5.0×10^6	6.3×10^{-5}	672	5.4×10^{-5}	9.0×10^6
s	0	3.0×10^{-5}	398	3.0×10^8	2.8×10^{-5}	3.0×10^8	2.7×10^{-5}	983	3.1×10^{-6}	3.0×10^8
s	1/2	3.0×10^{-5}	405	1.8×10^7	3.0×10^{-5}	1.2×10^8	2.7×10^{-5}	1265	4.7×10^{-7}	3.0×10^9

†Evaluated at 600 km altitude ($p = 1.5 \times 10^{-4}$ mbar, nominal model).

comparisons is in qualitative agreement with the results of *Parkinson et al.* [1990], who derived a value of 5×10^7 $cm^2\,s^{-1}$ for the eddy mixing coefficient at the helium homopause from a modeling analysis of UVS measurements of the 58.4 nm dayglow emission intensity, with the quoted uncertainties defining a range $0.6-16 \times 10^7$ $cm^2\,s^{-1}$. The acceptable values of K_h given in Tables 1 and 2 are generally smaller than the nominal value of Parkinson et al., but there are several reasons to expect this: first, the background atmosphere model adopted by Parkinson et al. is cooler overall than the nominal models used in this paper; second, as noted by *Bézard et al.* [1991], the helium homopause is generally located at altitudes above the methane homopause so that the corresponding value of K would be larger if eddy mixing becomes more vigorous with decreasing number density; third, Parkinson et al. neglected the incident 58.4 nm LISM flux in their modeling, leading to overestimates of He densities and K. (Note that the most plausible way to identify the homopause is as that altitude (or pressure level) where the time scale for diffusive transport equals the time scale for transport via mixing. At deeper levels, mixing is faster, while at higher altitudes, diffusive separation dominates. The molecular diffusion coefficient for CH_4 at $p \lesssim 1$ μbar in our p-T models is roughly half the He diffusion coefficient, hence one might expect helium to decouple from the H_2 background gas at a deeper pressure level than CH_4 — i.e., one might naively apply the $D = K$ rule and conclude that the He homopause must lie below the CH_4 homopause. The greater disparity in mass with H_2, however, results in CH_4 tending to relax to a diffusive equilibrium profile much more rapidly than He; this more than compensates for the smaller diffusion coefficient and leads to a deeper placement for the methane homopause.)

The dependence on temperature (specifically, the mean temperature at pressures 100–1 μbar) in inferring $f_T(CH_4)$ from the UVS lightcurves in our analysis is quite different from the dependence arising in the analysis of IR brightness spectra. Application of our UVS-derived $f_T(CH_4)$ constraints (along with realistic p-T profile forms) in the modeling of IR spectral measurements at 7–10 μm could provide a determination of atmospheric temperature near 0.1 mbar, in effect reversing the accustomed procedure wherein the p-T structure is prescribed and compatible $f_T(CH_4)$ values ascertained. Unfortunately, IRIS measurements have only set upper bounds on the abundance of methane. For our nominal p-T models, $T \approx 155$ K near 0.1 mbar (approximately the pressure level for the peak contribution to the CH_4 ν_4 emission escaping the atmosphere) and the corresponding IRIS upper limit for $f_T(CH_4)$ is 6×10^{-3}; increasing T(0.1 mbar) by 10 K reduces this to 4×10^{-4} (B. Bézard, private communication, 1991). The *Orton et al.* [1987, 1990] analyses of ground-based measurements of the methane ν_4 band emission relied on perturbed p-T models from *Appleby* [1986], with $T \approx 144$ K near 0.1 mbar (similar to the cool p-T models used in this paper). Increasing this temperature to 155 K lowers the methane abundance implied by the Orton et al. measurements from ~ 0.02 to $\sim 3 \times 10^{-3}$ [*Bézard et al.*, 1991]; a further 10 K increase in T(0.1 mbar) yields an even lower CH_4 abundance of $\sim 3 \times 10^{-4}$, consistent with the IRIS upper limits (B. Bézard et al., private communication, 1991). Clearly, use of our nominal and warm p-T models (or those of *Bézard et al.* [1991]) eases considerably the apparent discrepancy between the UVS-derived $f_T(CH_4)$ values and those advocated by Orton et al. Still, some disagreement remains, and the question also arises as to what might cause $T(p \lesssim 0.1$ mbar) to be so much warmer than predicted by *Appleby* [1986].

As a fortuitous circumstance, the UVS egress occultation occurred at the latitude of the tropopause temperature minimum revealed by IRIS measurements [*Conrath et al.*, 1991*b*]. Conrath et al. noted that the latitudinal variation in retrieved near-tropopause temperatures is reminiscent of the thermal structure seen at Uranus, hence the meridional circulation system implied by the IRIS measurements at Uranus [*Flasar et al.*, 1987] may be applicable to Neptune as well. In this circulation, the mid-latitude temperature minimum marks the zone of upwelling from the troposphere. *Yelle et al.* [1989], as part of an explanation for the apparent global subsaturation of methane in the Uranian stratosphere, invoked the Flasar et al. model and argued that the stratospheric abundance was limited by cold trap saturation at the temperature minimum. If this picture is carried over to Neptune, then the temperature minimum near 45°S latitude would define the reference cold trap value for $f_T(CH_4)$ (3×10^{-5}), in which case our modeling of the UVS data can be reconciled with cold trap saturation only if the stratosphere is distinctly warmer than our nominal p-T models, as discussed above. If, however, methane is injected into the stratosphere primarily via processes acting sporadically at localized sites (e.g., convective penetration from the upper troposphere), then the appropriate cold trap reference value of $f_T(CH_4)$ may refer to warmer tropopause regions ($T \gtrsim 55$ K).

In any event, our analysis of the UVS data points to the conclusion that if methane mixing ratios in the lower stratosphere do exceed cold trap values, it is by a factor of the order of 10 or less, not 1000. In separate pre-Voyager studies, *Lunine and Hunten* [1989] (LH) and *Stoker and Toon* [1989] (ST) sought to explain a stratospheric methane mixing ratio of 2% in terms of buoyant moist convection, with the idea that upwelling columns of gas originating near the base of the methane cloud deck might overshoot the tropopause and deposit CH_4 in the form of condensate particles directly into the lower stratosphere. Both LH and ST employed the one-dimensional steady-state entraining jet model of *Stoker* [1986], and both concluded that this extreme degree of supersaturation (with respect to cold trap values) might be explainable in these terms, subject to the verification of assumptions made regarding the upper tropospheric lapse rate, the strength of eddy mixing in the lower stratosphere, etc. LH assumed the temperature lapse rate in the region of cloud formation is roughly adiabatic or steeper, and argued that to initiate the formation of tropopause-penetrating convective "towers," either a dynamical mechanism must be acting over much of the planet to lift CH_4 cloud parcels above the cloud base a significant fraction of a scale height or there must be a modest degree of supersaturation (factor ~ 2) at the base of the methane cloud deck. The latter condition may be satisfied if there is a lack of suitable nuclei for heterogeneous nucleation, as seems to be the case [*Moses*, 1991]. LH also required $K > 10^4$ $cm^2\,s^{-1}$ in the lower stratosphere to ensure the lifting of 1 μm condensate particles to a level where evaporation would establish the desired 0.02 mixing ratio. ST criticized the LH scenario for relying on the presence of a methane cloud too thick to be consistent with observations and argued that moist convec-

tion initiated by the buoyancy of drier gas is more plausible and that invoking a large K in the lower stratosphere may be neither justifiable nor necessary. The scenarios presented by *Lunine and Hunten* [1989] and *Stoker and Toon* [1989] obviously need to be reassessed on the basis of Voyager findings. Upward transport of very small particles could account for the relatively weak degree of supersaturation consistent with our models, especially as the height at which evaporation would establish a value $\sim 10^{-4}$ for $f_T(CH_4)$ is $\lesssim 1$ scale height above the cold trap levels. In fact, given that the maximum supersaturations consistent with our UVS data-model comparisons correspond to saturation mixing ratios at pressures only ~1 scale height beneath the cold trap levels, where the temperature lapse rate is decreasing, then the instability of saturated atmospheric regions with weak-to-isothermal lapse rates to moist convection noted by both LH and ST may provide the basis of an adequate explanation. (It would then, however, be necessary to explain why this mechanism does not seem to apply to Uranus.)

In conclusion, our analysis of the UVS occultation data at wavelengths 125–138 nm indicates that past estimates of the methane abundance in the Neptune stratosphere are too high and that methane mixing ratios may in fact be consistent with cold trap saturation (within modeling uncertainties), depending on the manner by which CH_4 is introduced into the stratosphere. If the abundance of CH_4 is indeed limited by saturation, then the mean temperature at pressures 100–1 μbar may need to be increased over presently inferred values. The strength of eddy mixing in the 0.1–0.3 μbar region is fairly well prescribed by these model comparisons (roughly to within a factor of 3), which indicate that eddy mixing may be more vigorous at the egress latitude. The strength of eddy mixing at deeper pressure levels cannot be inferred from the present data-model comparisons. It is anticipated that modeling of the UVS lightcurves at longer wavelengths ($\gtrsim$ 140 nm) will yield some definitive information in this regard; these results will presented in a forthcoming paper.

Acknowledgements. We would like to express our appreciation to R. Wu for providing unpublished C_2H_2 and C_2H_4 EUV photoabsorption cross sections, to D. Hinson for providing us with material in advance of publication, to B. Bézard for discussions regarding the IRIS measurements, to R. Yelle for comments relating to an earlier manuscript, and to the referees for their comments. Research was supported by NASA grants NAGW-1504 (J.B.), NAGW-1771 (S.K.A.), NAS1-100 and NAGW-610 (B.R.S.), and NAGW-1498 (F.H.).

REFERENCES

Appleby, J. F., Radiative-convective equilibrium models of Uranus and Neptune, *Icarus*, *65*, 383–405, 1986.

Atreya, S. K., *Atmospheres and Ionospheres of the Outer Planets and Their Satellites*, Springer-Verlag, New York, 1986.

Baines, K. H., and W. H. Smith, The atmospheric structure and dynamical properties of Neptune derived from ground-based and IUE spectrophotometry, *Icarus*, *85*, 65–108, 1990.

Bézard, B., P. N. Romani, B. J. Conrath, and W. C. Maguire, Hydrocarbons in Neptune's stratosphere from Voyager infrared observations, *J. Geophys. Res.*, *96*, 18961–18975, 1991.

Bishop, J., S. K. Atreya, F. Herbert, and P. Romani, Reanalysis of Voyager 2 UVS occultations at Uranus: Hydrocarbon mixing ratios in the equatorial stratosphere, *Icarus*, *88*, 448–464, 1990.

Broadfoot, A. L., et al., Ultraviolet spectrometer experiment for the Voyager mission, *Space Sci. Rev.*, *21*, 183–205, 1977.

Broadfoot, A. L., B. R. Sandel, D. E. Shemansky, J. C. McConnell, G. R. Smith, J. B. Holberg, S. K. Atreya, T. M. Donahue, D. F. Strobel, and J. L. Bertaux, Overview of the Voyager ultraviolet spectrometry results through Jupiter encounter, *J. Geophys. Res.*, *86*, 8259–8284, 1981.

Broadfoot, A. L., et al., Ultraviolet spectrometer observations of Neptune and Triton, *Science*, *246*, 1459–1466, 1989.

Conrath, B., et al., Infrared observations of the Neptunian system, *Science*, *246*, 1454–1459, 1989.

Conrath, B. J., D. Gautier, G. F. Lindal, R. E. Samuelson, and W. A. Shaffer, The helium abundance of Neptune from Voyager measurements, *J. Geophys. Res.*, *96*, 18907–18919, 1991*a*.

Conrath, B. J., F. M. Flasar, and P. J. Gierasch, Thermal structure and dynamics of Neptune's atmosphere from Voyager measurements, *J. Geophys. Res.*, *96*, 18931–18939, 1991*b*.

Flasar, F. M., B. J. Conrath, P. J. Gierasch, and J. A. Pirraglia, Voyager infrared observations of Uranus' atmosphere: Thermal structure and dynamics, *J. Geophys. Res.*, *92*, 15011–15018, 1987.

French, R. G., J. H. Elias, D. J. Mink, and J. L. Elliot, The structure of Neptune's upper atmosphere: The stellar occultation of 24 May 1981, *Icarus*, *55*, 332–336, 1983.

French, R. G., et al., The 1983 June 15 occultation by Neptune. II. The oblateness of Neptune, *Astron. J.*, *90*, 2624–2638, 1985.

Hinson, D. P., and J. A. Magalhães, Equatorial waves in the stratosphere of Uranus, *Icarus*, *94*, 64–91, 1991.

Hubbard, W. B., et al., Results from observations of the 15 June 1983 occultation by the Neptune system, *Astron. J.*, *90*, 655–667, 1985.

Hubbard, W. B., et al., Oblateness, radius, and mean stratospheric temperature of Neptune from the 1985 August 20 occultation, *Icarus*, *72*, 635–646, 1987.

Hunten, D. M., Introduction and summary, in *The Atmosphere of Uranus: The Proceedings of a Workshop held at Ames Research Center September 30, 1974*, edited by D. M. Hunten, pp. 1–7, U.S. Government Printing Office, Washington, D.C., 1974.

Hunten, D. M., Vertical transport in atmospheres, in *Atmospheres of Earth and the Planets*, edited by B. M. McCormac, pp. 59–72, D. Reidel, Norwell, Mass., 1975.

Lee, L. C., and C. C. Chiang, Fluorescence yield from photodissociation of CH_4 at 1060–1420 Å, *J. Chem. Phys.*, *78*, 688–691, 1983.

Lindal, G. F., J. R. Lyons, D. N. Sweetnam, V. R. Eshleman, D. P. Hinson, and G. L. Tyler, The atmosphere of Neptune: Results of radio occultation measurements with the Voyager 2 spacecraft, *Geophys. Res. Lett.*, *17*, 1733–1736, 1990.

Lindzen, R. S., Tides and gravity waves in the upper atmosphere, in *Mesospheric Models and Related Experiments*, edited by G. Fiocco, pp. 122–130, D. Reidel, Norwell, Mass., 1971.

Lindzen, R. S., Turbulence and stress owing to gravity wave and tidal breakdown, *J. Geophys. Res.*, *86*, 9707–9714, 1981.

Lunine, J. I., and D. M. Hunten, Abundance of condensable species at planetary cold traps: The role of moist convection, *Planet. Space Sci.*, *37*, 151–166, 1989.

Moses, J. I., Photochemistry and Aerosol Formation in Neptune's Atmosphere, doctoral dissertation (Part II), Calif. Inst. of Technol., Pasadena, 1991.

Orton, G. S., and J. F. Appleby, Temperature structures and infrared-derived properties of the atmospheres of Uranus and Neptune, in *Uranus and Neptune*, edited by J. T. Bergstrahl, *NASA Conf. Pub. 2330*, 89–155, 1984.

Orton, G. S., D. K. Aitken, C. Smith, P. F. Roche, J. Caldwell, and R. Snyder, The spectra of Uranus and Neptune at 8–14 and 17–23 μm, *Icarus*, *70*, 1–12, 1987.

Orton, G. S., K. H. Baines, J. Caldwell, P. Romani, A. T. Tokunaga, and R. A. West, Calibration of the 7– to 14–μm brightness spectra of Uranus and Neptune, *Icarus*, *85*, 257–265, 1990.

Parkinson, C. D., J. C. McConnell, B. R. Sandel, R. V. Yelle, and A. L. Broadfoot, He 584 Å dayglow at Neptune, *Geophys. Res. Lett.*, *17*, 1709–1712, 1990.

Romani, P. N., and S. K. Atreya, Methane photochemistry and haze production on Neptune, *Icarus*, *74*, 424–445, 1988.

Romani, P. N., and S. K. Atreya, Stratospheric aerosols from CH_4 photochemistry on Neptune, *Geophys. Res. Lett.*, *16*, 941–944, 1989.

Smith, G. R., and D. M. Hunten, Study of planetary atmospheres

by absorptive occultations, *Rev. Geophys.*, *28*, 117–143, 1990.
Stoker, C. R., Moist convection: A mechanism for producing the vertical structure of the Jovian equatorial plumes, *Icarus*, *67*, 106–125, 1986.
Stoker, C. R., and O. B. Toon, Moist convection on Neptune, *Geophys. Res. Lett.*, *16*, 929–932, 1989.
Strobel, D. F., M. E. Summers, F. Herbert, and B. R. Sandel, The photochemistry of methane in the atmosphere of Triton, *Geophys. Res. Lett.*, *17*, 1729–1732, 1990.
Tyler, G. L., et al., Voyager radio science observations of Neptune and Triton, *Science*, *246*, 1466–1473, 1989.
Yelle, R. V., J. C. McConnell, D. F. Strobel, and L. R. Doose, The far ultraviolet reflection spectrum of Uranus: Results from the Voyager encounter, *Icarus*, *77*, 439–456, 1989.

S. K. Atreya, Department of Atmospheric, Oceanic and Space Sciences, University of Michigan, Ann Arbor MI 48109-2143.
J. Bishop, Computational Physics, Inc., 2750 Prosperity Avenue, Suite 600, Fairfax VA 22031.
F. Herbert and B. R. Sandel, Lunar and Planetary Laboratory, University of Arizona, Tucson AZ 85721.
P. N. Romani, Code 693.2, NASA Goddard Space Flight Center, Greenbelt MD 20771.

(Received February 12, 1991;
revised April 22, 1992;
accepted April 24, 1992.)